frontiers in Earth Science

ORIGINAL RESEARCH
published: 03 February 2022
doi: 10.3389/feart.2021.809839

An Investigation Into the Mechanism of Rock Bursts in Mines for Tunnel-Cut Isolated Areas with Multiple Stress Fields

Heng Zhang[1], Zhenhua Ouyang[2], Tie Li[1]*, Su Liu[3], Haiyang Yi[2], Honglei Wang[1], Jianqiang Chen[4] and Kang Li[4]*

[1]School of Civil and Resource Engineering, University of Science and Technology Beijing, Beijing, China, [2]School of Safety Regulation, North China Institute of Science and Technology, Langfang, China, [3]School of Resources and Civil Engineering, Northeastern University, Shenyang, China, [4]Shenhua Xinjiang Energy Co., Ltd., Urumchi, China

Tunnels in several mines in Shaanxi Province, China, which are subject to multiple stress fields, are used as case studies to clarify the structural problems associated with rock bursts that occur in high-stress mines. Field studies featuring field measurements and theoretical analysis are used to investigate the modes and mechanisms of failure. The following are the main findings: (1) a model for distributing the dominant pressure features around the goaf was established by analyzing the stress distribution induced by the goafs on both sides of the excavated zone in a coal seam. The model reveals the pressure distribution in the tunnel-cut area, which is the mechanical factor responsible for rockburst. (2) Because of the goafs acting on both sides of the tunnel, an area of concentrated stress was formed, and stress was transferred to the coal seam. The intense tunnel-cutting action can reduce the stability of the coal. The plastic area caused by tunnel mining and a reduction in the elastic area of the tunnel-cut coal pillars in each segment, increase the possibility for rockburst under the application of dynamic-static stress; this process is known as a stabilizing factor. (3) Due to the combined effect of the tunnel-cut and goafs on both sides, most of the microseismic incidents happened in the core area of coal pillar and in the side of tunnels. When the stress applied on coal pillar is more than critical strength, burst and mine earthquake can be induced. Our study focused mainly on rockburst incidents that occurred in coal mines in Shaanxi Province, which were caused by tunnel-cut coal seams that were subject to multiple stress fields. The study has direct implications for developing new and improved guidelines for preventing rockburst in mines.

Keywords: roadway, rock burst prevention, stress field, coal cutting, stress concentration

OPEN ACCESS

Edited by:
Jinyang Fan,
Chongqing University, China

Reviewed by:
Xuyao Qi,
China University of Mining and Technology, China
Wenyu Lv,
Xi'an University of Science and Technology, China

****Correspondence:***
Zhenhua Ouyang
oyzhua@163.com
Tie Li
litie@ustb.edu.cn

Specialty section:
This article was submitted to Geohazards and Georisks, a section of the journal Frontiers in Earth Science

Received: *05 November 2021*
Accepted: *27 December 2021*
Published: *03 February 2022*

Citation:
Zhang H, Ouyang Z, Li T, Liu S, Yi H, Wang H, Chen J and Li K (2022) An Investigation Into the Mechanism of Rock Bursts in Mines for Tunnel-Cut Isolated Areas with Multiple Stress Fields. Front. Earth Sci. 9:809839. doi: 10.3389/feart.2021.809839

INTRODUCTION

When a large amount of energy is stored in abandoned mines, it has a great impact on the safety of underground coal mines, resulting in the occurrence of rock burst accidents (Jiang et al., 2016; Fan et al., 2020; Liu et al., 2020a; Kang et al., 2021). Rock bursts, which can occur in mining are well known in the industry and can threaten mine safety (Ma et al., 2015; Barton and Shen, 2017; Keneti and Sainbury, 2018; Rehman et al., 2021; Xiong et al., 2021). A rockburst is typically influenced by geological conditions and the mining technology used (Jiang et al., 2014; Qi et al., 2020; Qi et al.,

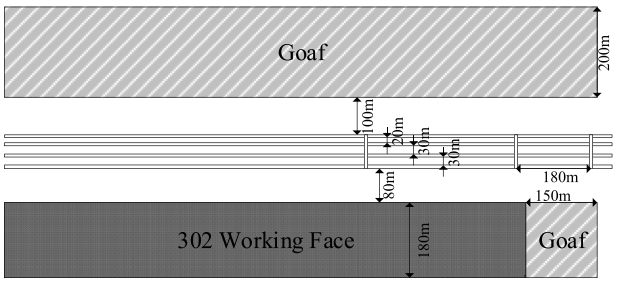

FIGURE 1 | Layout of roadways and working faces on both sides of the island area.

Thickness	Columnar	Lithology	Lithology
73.3 m		Fine sandstone mudstone fine sandstone mudstone	Fine sandstone group with argillaceous intercalation, single layer thickness less than 10m. Mudstone: light gray, maroon, hard, containing sandy argillaceous breccia. Fine sandstone: gray, dark gray, massive, containing a large number of plant fossils, locally containing a small amount of calcite vein, with sliding surface in the upper part, and obvious contact with the underlying. Some of them are intercalated with medium grained sandstone.
3.8 m		Coarse grained sandstone	Gray, mainly composed of quartz and feldspar, well sorted, sub round, argillaceous cementation, wavy bedding, intercalated with thin layer of siltstone, local containing siderite nodules, and obvious contact with underlying. 4 coal black weak pitch luster, black streaks, ladder shaped fault, banded structure, with endogenous fissures, a small amount of vitrinite composed of bright coal and dark coal, a huge thick coal seam with simple structure.
23.9 m		mudstone	Gray, dark gray, massive, containing a large number of plant fossils, locally containing a small amount of calcite veins, with sliding surface in the upper part, and obvious contact with the underlying. Gray, mainly composed of quartz and feldspar, well sorted, sub round, argillaceous cementation, wavy bedding, intercalated with thin layer of siltstone, local containing siderite nodules, and obvious contact with underlying.
15.9 m		4 coal	4 coal black weak pitch luster, black streaks, ladder shaped fault, banded structure, with endogenous fissures, a small amount of vitrinite composed of bright coal and dark coal, a huge thick coal seam with simple structure.
4.5 m		mudstone	It is light gray and dense, containing plant root fossils, and sliding surface can be seen at the broken place.
3.0 m		Fine-grained sandstone	Light gray, maroon, hard, with sandy argillaceous breccia.

FIGURE 2 | Histogram for working face of a coal mine.

2019; Liu et al., 2020b; Zhang et al., 2021a). Many rockburst accidents have occurred as mining depths have increased, resulting in numerous casualties and damage to equipment and infrastructure (Dou et al., 2003; Pan et al., 2003; Pan et al., 2012; Fan et al., 2019; Jiang et al., 2021; Li et al., 2021). On October 20, 2018, a serious rockburst incident occurred in Shandong Province (Shandong Energy Dragon Mine Group, Longyun Coal Industry Co., Ltd.), resulting in 21 deaths and four injuries. On August 2, 2019, a dynamic event occurred in the connecting tunnel (F5010) around a coal pillar while 12 workers were cleaning the tunnel, resulting in seven fatalities. Another accident occurred on February 22, 2020, in the Xinjulong mine in Shandong, resulting in four deaths and the loss of 18 million RMB. In the aforementioned incidents, the tunnel-cut coal areas were subjected to the lateral abutment pressure of the goafs and mining stress in the working face, which affected the associated geological structures and accumulated a significant amount of strain energy in the areas in question (Cui et al., 2021; Liu et al., 2021; Tian et al., 2021; Wu et al., 2021). Therefore, failure of overlying strata readily occurred over a wide area, resulting in rock bursts.

Wang et al. (2019) elaborated on the principles of failure for isolated coal seams in a tunnel in a deep mine and proposed a mechanism and a failure model for the coal under reduced pressure. Zhao et al. (2018) demonstrated that the stability of a coal pillar is mainly determined by the movement of the overlying strata in the goaf and by repeated mining; a practical method to evaluate the width of the coal pillar was also proposed. Feng et al. (2015) investigated an elastic bearing area and developed a model for the abutment pressure applied to an isolated working face. Song et al. (2018) outlined the principles of failure due to creep in an isolated coal pillar over time and obtained the conditions of failure for the entire working face. Chen et al. (2012) investigated the conditions of a stripe coal pillar under pressure over a long period and discovered that the coal pillar can be divided into three parts, i.e., an elastic area, a plastic area, and a failed area. Lu and Guo (1991) investigated the relationship between the deformation of the surrounding rocks and the width of the coal pillar. Jiang et al. (2018) used tectonic stress to determine the width of the coal pillar based on inverse analysis of *in situ* stress and numerical modeling. Li et al. (2013) used theoretical analyses and modeling to study the mechanical mechanism of rockburst based on the surrounding rock stress by monitoring microseismic activities and field data. Zheng et al. (2012) reviewed the laws of stress distribution of coal pillars in gob-side mining at different widths by combining theoretical and numerical analysis and proposed that the width of the coal pillar can be affected by disturbances caused by tunnels in the mine and advanced mining practices. Yang et al. (2017) proposed a method for determining the width of a coal pillar by analyzing the creep data. Yin et al. (2012) used theoretical analysis and numerical modeling to investigate the size of the protected dip coal pillar in joint mining areas. Wang and Miao (2007) used mechanical analysis to conduct topotactic transformation studies on the conditions of a coal pillar failure and obtained the probability function for failure. Wang et al. (2009) developed a mechanical model for the residual coal pillar in the lower protective strata. Li et al. (2020) investigated the mechanism of rockburst caused by a coal pillar, developed a computational model of the overlying loading by the strata on the coal pillar, and assessed the risk of rockburst for the entire pillar. Jiang et al. (2015) proposed a system in the context of coal seam failure and noted that when the stress loading on the coal seam is greater than 1.5 times the uniaxial compressive strength, a rock burst will occur.

Several studies have been conducted to prevent the occurrence of a rockburst in an isolated coal pocket or pillar (Adoko et al., 2013; Xu et al., 2017; Zhou et al., 2018; Pinzani and Coli, 2011; Zhang et al., 2021b; Liu et al., 2021), but little research has focused on the types of rock bursts that can occur in tunnel-cut coal. This study focuses on several incidents that have occurred in Shaanxi Province. We investigated the features of stress distribution and variation in the elastic area under the action of tunnel cutting,

FIGURE 3 | Photographs of the rockburst event.

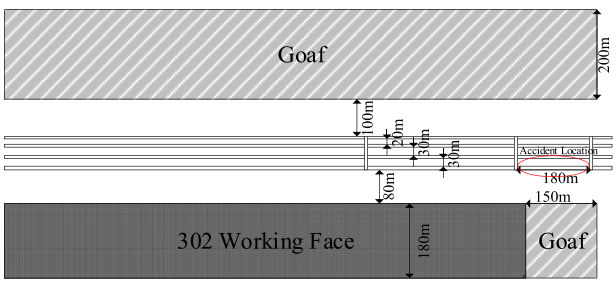

FIGURE 4 | Schematic of the location of the incident.

whereby both sides of the tunnel are goafs, clarifying the mechanical mechanism for the rockburst and failure of the coal pillar, which is subject to combined multiple stress fields. The risk of a rockburst that occurs in a mine and some preventative measures to avoid it are also elaborated.

CASE STUDIES

General Introduction to the Working Face

There are four tunnels 100 m south of goafs 204, 205, and 206, including the west-wing haulage roadway, the second section of the air-inlet roadway, the belt roadway, and the air-return roadway with gaps of 20, 30, and 30 m between each roadway, respectively. The working face of mine 302, which is 180 m wide, is located 80 m south of the air-return roadway (**Figure 1**). The coal seam is 590.5 m deep and the overlying layers within 100 m are less than 10 m thick, with a uniaxial compressive strength of <60 MPa. The overlying strata consist of sandstone and mudstone (**Figure 2**). The coal seam has a dip angle of 4 and a uniaxial compressive strength of 15 MPa. The floor of the coal seam consists of coarse-grain sandstone, mudstone, and fine-grain sandstone. The test results show that the coal seam and roof strata are prone to failure because of rockburst, whereas the reverse is true for floor strata.

The Incident

On February 25, 2017, the belt roadway, the air-return roadway, and the connecting roadways experienced gunite-layer cracking, cracking of the walls and roof, the heaving of the floor and walls, and deformation because of the combined effects of the lateral abutment pressure from three consecutive goafs (204, 205, and 206), as well as the lateral abutment pressure from the working face 302 and the mining stress; this resulted in significant damage to the tunnel support systems, with roof protrusion of up to 1 m at a maximum. All the roadways were set inside the coal seam. Photographs of the damage caused by the rockburst are shown in **Figure 3** and the exact locations are shown in **Figure 4**.

Microseismic Monitoring and Analysis

The tunnel-cut coal pillar has experienced a dense distribution of microseismic events over time because it has been subjected to stress from the lateral goaf, the cutting tunnel, and the working face of the mine. **Figure 5** is a schematic of microseismic monitoring points and the locations of the events. Three mobile sites for microseismic

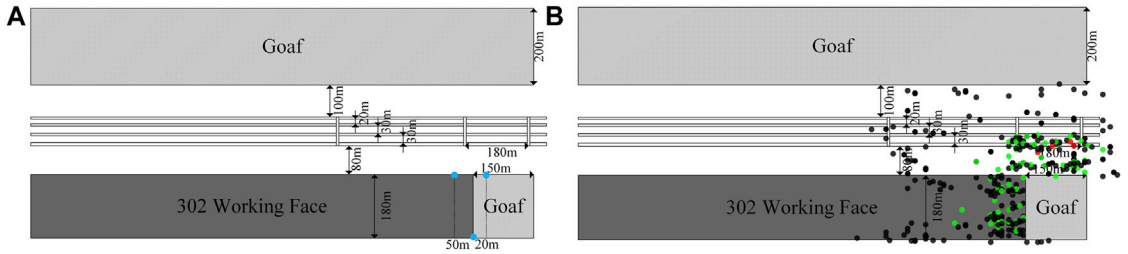

FIGURE 5 | Schematic of microseismic monitoring points and the locations of the events.

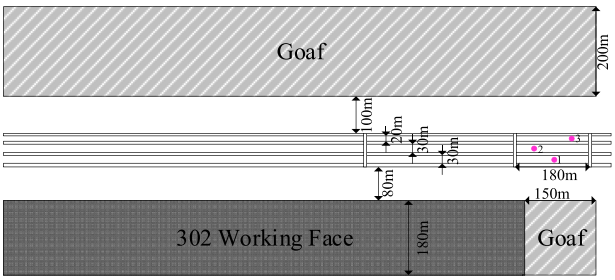

FIGURE 6 | Ground displacement monitoring points.

monitoring were located in the working face 302 (**Figure 5A**), one in the air-return roadway and one in the air-inlet roadway, each with a horizontal separation distance of 20 m; another was located in the air-inlet roadway, which was situated 50 m ahead of the working face. The black circles in **Figure 5A** represent microseismic events with an order of magnitude of 10^2 *J* or less, whereas the green circles represent events of magnitude 10^3 *J*, and the red circles represent events of magnitude 10^4 *J*. **Figure 5B** shows that numerous microseismic events occurred in the roadways and in the front of the working face, especially at the side close to the working face 302. The tunnel-cut isolated area featured a dense distribution of microseismic events of a large order of magnitude, indicating that the rock system retained a massive amount of elastic energy, with the tunnels cutting through the isolated area. The lateral abutment pressure and tunnel-cutting behavior resulted in energy accumulation and a concentration of stress in the isolated area in the mining of the working face. When the abutment pressure reached a critical level, the coal-rock mass fails, releasing a significant amount of energy and causing a rockburst.

Monitoring of Ground Surface Settlement and Analysis

The ground surface settlement was monitored in the air-return roadway, belt roadway, the second section of the air-inlet roadway, and the isolated area cut by the west-wing tunnel (**Figure 6**). Based on the monitoring of the working face 302, the surface settlement curve is shown in **Figure 7**. This figure showed that in March 2016, the accumulated settlements at monitoring points 1, 2, and 3 were 33.5, 58, and 72.3 mm, respectively; additionally, the average settlement rates for each isolated area were 1.12, 1.93, and 2.41 mm/ d, respectively, indicating that the ground surface settled steadily. The settlements for the three locations in March 2017 are indicated in **Figure 7B**. The settlements corresponding to the air-return roadway, belt roadway, the second segment of the air-inlet roadway, and the isolated area cut by the west-wing tunnel correspond to displacements of 295, 146.5, and 102.1 mm, respectively. The maximum settlement for monitoring point 1 was 200 mm on March 25 with a rate of 200 m/d, which was approximately 178 times the previous rate (**Figure 7A**). In conclusion, as the overlying strata over the goafs and working face move, disturbances in the overlying strata of the tunnel-cut area are induced, resulting in the ground surface settlement.

Monitoring the ground surface settlement revealed that the constant movement of the strata on the goaf and the working face causes movement of the strata on the tunnel-cut isolated coal seam, resulting in massive loading of the roof with subsequent heaving, cracking, and deformation of the supporting beams in the tunnels.

Stress Monitoring and Analysis

Stress gauges were installed in the air-return roadway, belt roadway, the second section of the air-inlet roadway, and the railway (for transport) in the west wing. The gauges were numbered 1#, 2#, 3#, and 4#. The stress values in March 2016 and 2017 are shown in **Figure 8**, indicating that the average stress values for the air-return roadway, belt roadway, the second section of the air-inlet roadway, and the railway in the west wing in March 2016 were 4.33, 4.50, 4.46, and 4.47 MPa, respectively, with all values increased significantly in March 2017 (**Figure 8**). For example, the stress value for gauge 1 (**Figure 8A**) reached 9.39 MPa, more than double of the previous year. The lateral abutment pressure from the goaf, the tunnel-cut action, the constant settlement of the overlying strata over the goaf, and the mining working face ultimately affected the roadways, resulting in deformation and failure of the roadways and support systems.

FAILURE MECHANISM IN THE ISOLATED AREA WITH COMBINED MULTIPLE STRESS FIELDS

Mechanical Mode for the Lateral Abutment Pressure

As the working face are mined, goafs are formed on both sides of the tunnel-cut coal pillar. An isolated coal pillar is shown in **Figure 9A**, while the stress transfer in the isolated coal pillar is

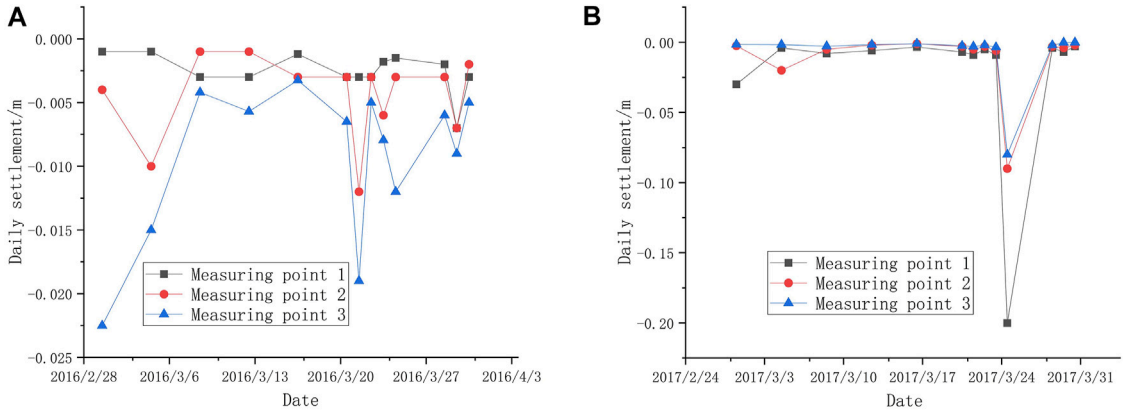

FIGURE 7 | Surface settlement curve.

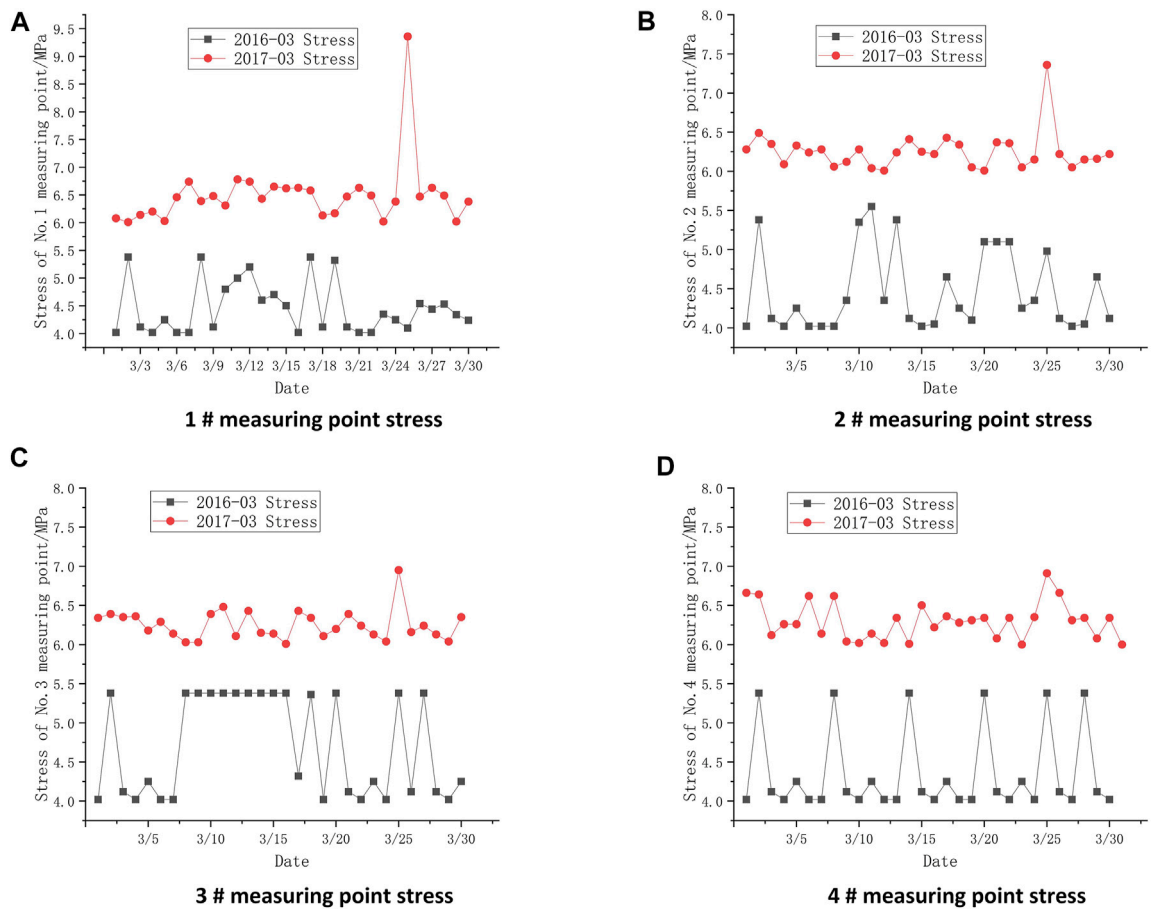

FIGURE 8 | Stress curve diagrams for each main roadway. **(A)** 1 # measuring point stress, **(B)** 2 # measuring point stress, **(C)** 3 # measuring point stress, and **(D)** 4 # measuring point stress

shown in **Figure 9B**. Stress transfer occurred as goafs are formed on both sides and the overlying strata move with the geostatic stress of the isolated coal pillar. The peak of the stress curve moved toward the isolated coal pillar from the goaf and stress was transferred to the isolated coal pillar below, changing the stress distribution in the isolated coal pillar.

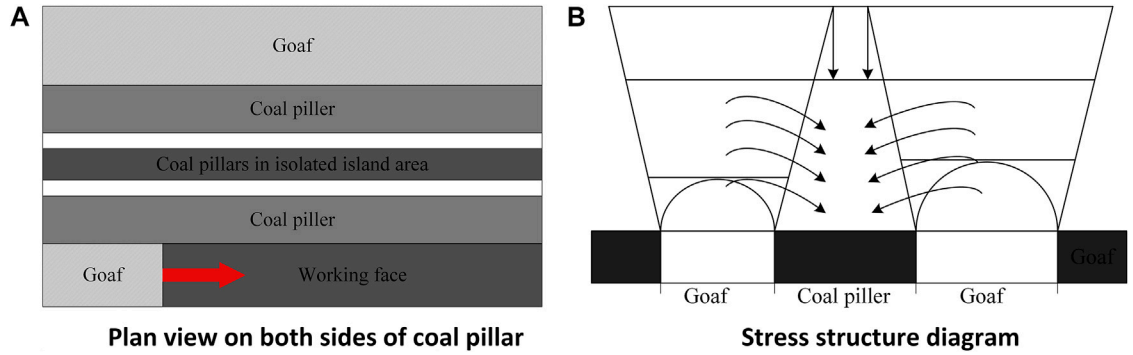

FIGURE 9 | Distribution characteristics of superimposed stress field after the formation of the goaf on both sides of the coal pillar island area. **(A)** Plan view on both sides of coal pillar, and **(B)** Stress structure diagram

The isolated coal pillars in the goafs were imposed by the transfer of stress from the excavated zone, the suspended strata, and the geostatic stress of the topsoil (σ_i, σ_m, σ_Z) (**Figure 11**). For simplicity, a model of complete settlement in the goafs was assumed to operate. The stresses applied on the coal pillar consisted of three parts, such as the gravity of the excavated zone (σ_i), half pressure from the suspended rock zone (σ_m), and gravity due to the overlying topsoil (σ_Z). The combined stresses from multiple fields in the goafs were applied to the coal pillar, resulting in a cumulative stress equation, which is written as the following:

$$\sigma = \sigma_z + \sigma_m + \sigma_i \tag{1}$$

The geostatic stress of the overlying topsoil is:

$$\sigma_z = \begin{cases} \dfrac{\gamma H \tan\eta}{2h_1 + h_2} x_1 + \dfrac{\gamma H \tan\varepsilon}{2n_1 + n_2} x_2 \, x_1 \left[0, \dfrac{2h_1 + h_2}{\tan\eta}\right], x_2 \left[0, \dfrac{2n_1 + n_2}{\tan\varepsilon}\right] \\ \gamma H_1 + \gamma H_2 \quad H_1 \left[\dfrac{2h_1 + h_2}{\tan\eta}, +\infty\right], H_2 \left[\dfrac{2n_1 + n_2}{\tan\varepsilon}, +\infty\right] \end{cases} \tag{2}$$

and stress from the suspended rock zone is

$$\sigma_m = \begin{cases} \dfrac{2\sigma_{m1max} x_1 \tan\eta}{2h_1 + h_2} + \dfrac{2\sigma_{m2max} x2 \tan\varepsilon}{2n_1 + n_2} \quad x_1 \left[0, \dfrac{2h_1 + h_2}{2\tan\eta}\right] \\ , x_2 \left[0, \dfrac{2n_1 + n_2}{2\tan\varepsilon}\right] \sigma_{m1max} \left(2 - \dfrac{2x_1 \tan\eta}{2h_1 + h_2}\right) \\ + \sigma_{m2max} \left(2 - \dfrac{2x_2 \tan\varepsilon}{2n_1 + n_2}\right) x_1 \left[\dfrac{2h_1 + h_2}{2\tan\eta}, \dfrac{2h_1 + h_2}{\tan\eta}\right] 0 \\ x_1 \left(\dfrac{2h_1 + h_2}{\tan\eta}, +\infty\right), x_2 \left(\dfrac{2n_1 + n_2}{\tan\varepsilon}, +\infty\right), x_2 \left[\dfrac{2n_1 + n_2}{2\tan\varepsilon}, \dfrac{2n_1 + n_2}{\tan\varepsilon}\right] 0 \end{cases} \tag{3}$$

where σ_{m1max} and σ_{m2max} can be expressed as the following:

$$\sigma_{m1max} = \frac{\left[\left(\frac{L1}{2} + \frac{2h_1 + h_2}{2\tan\eta}\right) h_2 + \left(\frac{L1}{2} + \frac{h_1 + h_2}{\tan\eta}\right) h_3\right] \gamma}{(2h_1 + h_2)\cot\eta} \tag{4}$$

$$\sigma_{m2max} = \frac{\left[\left(\frac{L2}{2} + \frac{2n_1 + n_2}{2\tan\varepsilon}\right) n_2 + \left(\frac{L2}{2} + \frac{n_1 + n_2}{\tan\varepsilon}\right) n_3\right] \gamma}{(2n_1 + n_2)\cot\varepsilon} \tag{5}$$

Stress from the excavated zone may be written as the following:

$$\sigma_i = \begin{cases} \dfrac{2\sigma_{i1max} x_1 \tan\eta}{h_1} + \dfrac{2\sigma_{i2max} x2 \tan\varepsilon}{n_1} \quad x_1 \left[0, \dfrac{h_1}{2\tan\eta}\right] \\ , x_2 \left[0, \dfrac{n_1}{2\tan\varepsilon}\right] 2\sigma_{i1max} \left(1 - \dfrac{x_1 \tan\eta}{h_1}\right) + 2\sigma_{i2max} \\ \left(1 - \dfrac{x_2 \tan\varepsilon}{n_1}\right) x_1 \left[\dfrac{h_1}{2\tan\eta}, \dfrac{h_1}{\tan\eta}\right], 0 \; x_1 \left(\dfrac{h_1}{\tan\eta}, +\infty\right), \\ x_2 \left(\dfrac{n_1}{\tan\varepsilon}, +\infty\right) x_2 \left[\dfrac{n_1}{2\tan\varepsilon}, \dfrac{n_1}{\tan\varepsilon}\right] \end{cases} \tag{6}$$

where σ_{i1max} *and* σ_{i2max} can be expressed as the following:

$$\sigma_{i1max} = \left(\frac{L_1 \tan\eta}{4} + \frac{h_1}{2}\right) \gamma K_{i1} \tag{7}$$

$$\sigma_{i2max} = \left(\frac{L_2 \tan\varepsilon}{4} + \frac{n_1}{2}\right) \gamma K_{i2} \tag{8}$$

In **Eqs 1–8** and **Figure 10** H is the depth of mining, and h_1, h_2, h_3, n_1, n_2, and n_3 are the strata heights in the three zones; η, *and* ε are the excavation angles; x_1 and x_2 are the goaf-affected distances in the lateral side; σ_{m1max}, σ_{m2max}, σ_{i1max}, *and* σ_{i2max} are the peak values of transfer stresses from the excavated zone and the suspended zone, respectively. L_1 and L_2 are the widths of the goafs, D_1, D_2, and D_3 are the widths of the coal pillars in the different areas of the goaf on both sides. K_{i1} and K_{i2} are the stress transfer coefficients in the excavated zone.

The equations above only considered the transfer stress from the three zones in the goafs and the geostatic stress of the overlying strata. The isolated coal pillar was also affected by mining-induced stresses in the roadway, at the working face, and the geological structure, which would have increased the degree of stress concentration in the area. The sum of the lateral abutment pressure is given by the following:

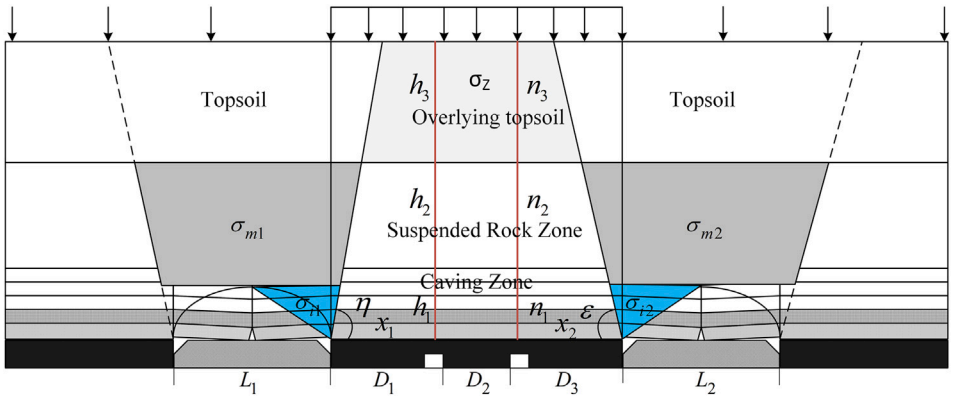

FIGURE 10 | Theoretical analysis model of the coal stress structure field in the area of the goaf islands on both sides of the excavated zone.

$$\sigma_T = \lambda\sigma \tag{9}$$

where λ is the coefficient of stress concentration caused by multiple factors, the value usually varies between 1 and 1.5. By analyzing the above equations, and combining them with the values of x_1 and x_2, the solution for distributing stress for the abutment pressure on the coal pillar D_2 can be obtained.

Action by Goafs on Both Sides of the Excavated Zone

The parameters for the goafs and the working face 302 include the following: L_1 = 200 m, L_2 = 180 m, D_1 = 130 m, D_2 = 30 m, D_3 = 80 m, $\eta = \varepsilon = 71^{\circ}$, and H = 590.5 m. The height of the working face was 3.8 m, and the unit weight of the rock is γ = 25 KN/m^2. Given that the working face 302 has been mined to a depth of 150 m, which was greater than the size of squaring, leads to complete settlement in the goafs. Therefore, we can substitute $h_1 = n_1$ = 38 m, $h_2 = n_2$ = 200 m, and $h_3 = n_3$ = 352.5 m into **Eqs 1–9**.

Transfer of the geostatic stress from the overlying topsoil can be expressed as a step function as follows:

$$\sigma_z = \begin{cases} 0.155\,(x_1 + x_2) & x_1, x_2\,(0, 95.2) \\ 0 & x_1, x_2\,(95.2, +\infty) \end{cases} \tag{10}$$

Transfer of the stress from the suspended rock zone:

$$\sigma_m = \begin{cases} 0.525x_1 + 0.494x_2 & x_1, x_2\,(0, 47.6) \\ (49.922 - 0.524x_1) + (46.978 - 0.493x_2) & x_1, x_2\,(47.6, 95.2) \\ 0 & x_1, x_2\,(95.2, +\infty) \end{cases} \tag{11}$$

Transfer of stress from the excavated zone:

$$\sigma_i = \begin{cases} 0.688x_1 + 0.627x_2 & x_1, x_2\,(0, 6.5) \\ (9.02 - 0.688\mathrm{x}_1) + (8.22 - 0.627x_2) & x_1, x_2\,(6.5, 13.1) \\ 0 & x_1, x_2\,(13.1, +\infty) \end{cases} \tag{12}$$

In summary, the combined multiple stress fields acting on the coal pillar from the goafs on both sides can be expressed as:

$$\sigma_T = \lambda\sigma = \begin{cases} 1.368\mathrm{x}_1 + 1.276\mathrm{x}_2 & \mathrm{x}_1, \mathrm{x}_2\,(0, 6.5) \\ (9.02 - 0.008\mathrm{x}_1) + (8.22 + 0.022\mathrm{x}_2) & \mathrm{x}_1, \mathrm{x}_2\,(6.5, 13.1) \\ 0.68\mathrm{x}_1 + 0.649\mathrm{x}_2 & \mathrm{x}_1, \mathrm{x}_2\,(13.1, 47.6) \\ (49.922 - 0.369x_1) + (46.978 - 0.338x_2) & x_1, x_2\,(47.6, 95.2) \\ 0 & x_1, x_2\,(95.2, +\infty) \end{cases} \tag{13}$$

where λ is set as 1.4 by considering the coal residing in the tunnels, the working face, and the geological structure. According to the above equations, the graph of the lateral abutment pressure in the goafs corresponds to that shown in **Figures 11**, **12**.

Because the action and mechanical mechanism of the goaf on both sides of the roadway on the coal pillar cutting area are the same, **Figures 11**, **12** show that the two lateral influence pressure diagrams are similar, and the maximum range of lateral supporting stress on both sides of the goaf is 95.2 m. The stress peak area is located at 47.6 m from the coal wall of the goaf. **Figure 11A** shows that the peak value of lateral supporting stress applied to coal pillar in goaf 204, 205, 206 is 45.32 MPa. As shown in **Figure 11B**, the peak value of lateral supporting stress in goaf 302 is 43.2 MPa. The lateral side of goafs 204, 205, and 206 was 150 m to the coal pillar (**Figure 12**), which was cut by the belt roadway and the air-return roadway, and the distance was more than the maximum lateral affecting range (95.2 m), where the wall of goaf 302 was 80 m to the coal pillar cut by the air-inlet and belt roadways. Therefore, the coal pillar (D_2) was affected only by the transfer stress from goaf 302. The isolated coal pillar between 80 and 95.2 m, the air-return roadway, and the connecting tunnel experience a high concentration of stress (**Figures 11B**, **12**).

The index used to assess the likelihood of a rockburst is given by the following:

$$I_c = \sigma_T/\sigma_c \tag{14}$$

where σ_T is the total stress applied to the coal seam, and σ_c is the uniaxial compressive strength of the coal. Based on **Table 1**, **Figures 11B**, **12**, and **Eq. 14**, the coal beyond 24–92 m was subject to the stress of 1.5 times the uniaxial compressive strength imposed by the goaf and there was no risk of a rockburst, but if the coal body was within this range (24–92 m), the index would be greater than 1.5.

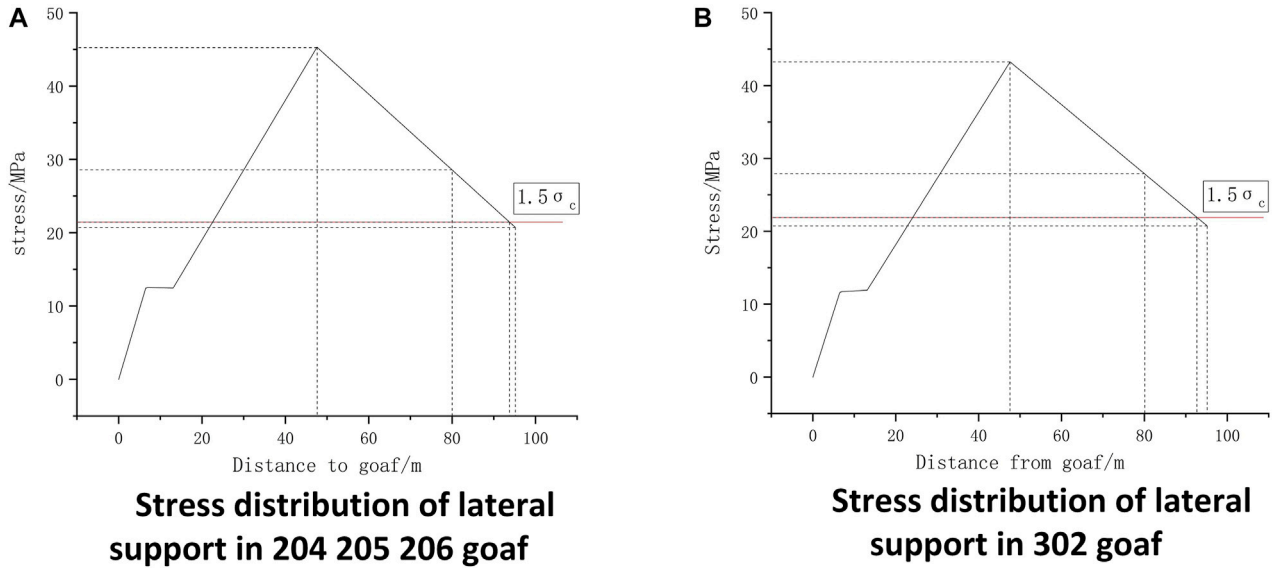

FIGURE 11 | Stress distribution diagram of lateral support. **(A)** Stress distribution of lateral support in 204 205 206 goaf, and **(B)** Stress distribution of lateral support in 302 goaf

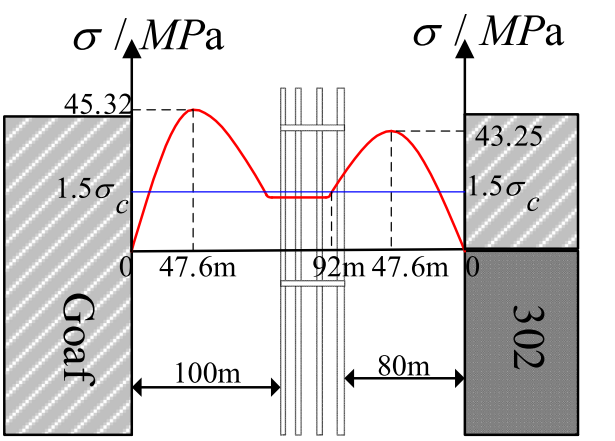

FIGURE 12 | Effect of the supporting stress in the goaf on both sides.

Particularly, all rockburst indices for the coal pillar, the air-return roadway, and the connecting tunnel were greater than 1.5, which can significantly induce a rockburst. The tunnels-cut isolated coal pillar, the tunnels, and the connecting tunnels were subject to a state of high-stress concentration. Significantly, the distance between the isolated coal pillar and the goaf was inadequate because of the high probability of rockburst in the tunnels and connecting tunnel, so rockburst incidents were likely.

Analysis of the Stability of Tunnel-Cut Coal

To study the stability of an isolated coal seam cut by tunnels, a model with a size of 100*1*100 m was established based on the actual geological conditions. The following are the boundary conditions; the bottom and the four sides were fixed, and the top was free. Geostatic stress was applied to the top of the model. The model included 120,800 nodes, 5,800 elements, and the space between the tunnels was set as 30 m. The parameters for the properties of the coal-rock body are listed in **Table 2**.

TABLE 1 | Risk level.

No impact	Weak shock	Medium impact	Strong impact
0.0 – 1.5	1.5–2.0	2.0–2.5	2.5 above

Figure 13 shows a 20-m gap between the tunnels, and the coal cut by the tunnels is subject to a concentration of stress, with a peak value of up to 23.15 MPa. According to the rockburst index, a rock burst would occur when the stress applied to the coal was greater than 1.5 times the uniaxial compressive strength ($\sigma_c >$ 22.5 MPa).

Figure 14 shows that the distance between the tunnels is 30 m. The isolated coal pillar, the roof, the walls, and the floor are displaced during the mining process; the maximum displacement of the roof was 19 mm; the walls on both sides had maximum displacements of 17 mm; the displacement of the floor was 9 mm; The displacement of the middle coal pillar is approximately 1–7 mm, the position movement and deformation of the coal and rock mass around the cutting coal pillar, and the roadway are broken, and the integrity of the coal pillar and coal-rock mass is poor, and the stability of the coal pillar is reduced.

Figure 15 shows that when the roadway spacing is 30 m. Shear and tensile failure occurred around the roadway during the mining process, a large plastic failure area appears in the cutting coal pillar and roadway surrounding rock, the stress-bearing limit is reduced, and the elastic zone is reduced to the central area of the coal pillar.

In summary, tunnel cutting while mining reduced the stability of the coal pillar and redistributed stress on the isolated coal

TABLE 2 | Material properties.

Material properties / Lithology	Bulk modulus/GPa	Shear modulus/GPa	Internal friction angle	Cohesion/MPa	Tensile strength/MPa
Soft sandstone	10.8	5.7	31.65	3.43	2.0
Mudstone	6.6	4.9	28.54	2.45	1.0
Grade 4 coal	5.5	3.8	25.66	1.44	0.5
Hard sandstone	11.6	6.6	33.53	3.76	2.5

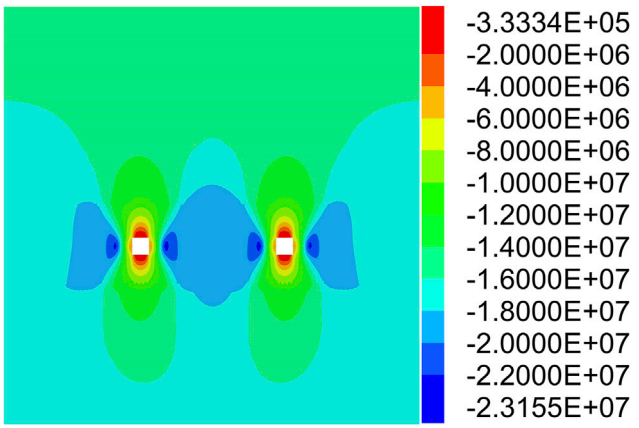

FIGURE 13 | Cloud diagram for the vertical stress distribution (Pa).

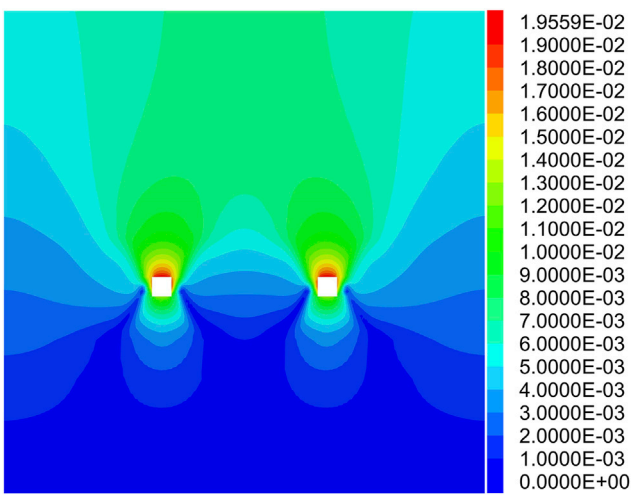

FIGURE 14 | Displacement nephogram (m).

pillar; simultaneously, the stress began to be transferred to the middle of the coal pillar, resulting in stress concentration on both sides of the tunnel-cut isolated coal seam. The rockburst index was greater than 1.5, indicating that the coal pillar was prone to fracture. Meanwhile, the plastic area in the coal pillar increased while the elastic area decreased, reducing the elastic strain energy. An intense concentration of stress developed on both sides of the goaf and the working face, causing the combined dynamic-static stress to cause a rockburst.

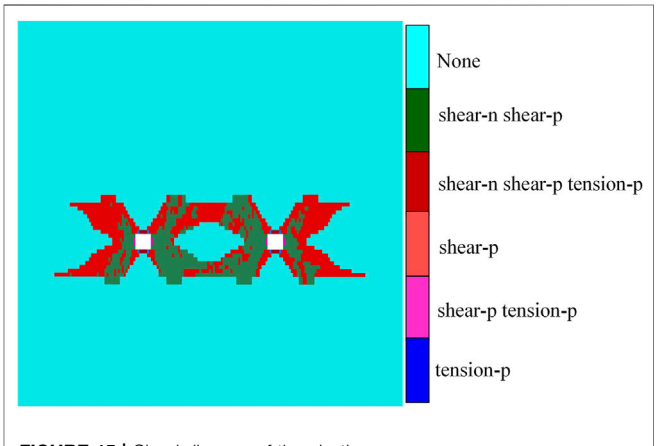

FIGURE 15 | Cloud diagram of the plastic zone.

DISCUSSION

Mechanical analysis and numerical modeling studies have been conducted to clarify the mechanism of tunnel-cut induced rock bursts and to identify measures that can avoid or at least minimize the incidence of rock bursts in coal mining. The following key measures must be implemented: arranging a reasonable gap between the isolated coal pillar and the goafs on both sides; arranging for a reasonable distance between tunnels; increasing the compressive strength of isolated coal pillars; increasing the strength of tunnels; strengthening the monitoring and warning systems in the mines.

1) Arranging a reasonable distance between the tunnel-cut isolated coal pillar and the goaf

According to **Eq. 14** and **Figures 11**, **12**, the stress applied to an isolated coal pillar cut by a tunnel increased and then decreased with distance to the goaf; the distance of goaf 302 to the isolated coal pillar was 80 m, which was within the range of stress concentration. To avoid a rockburst, we must set a reasonable distance between the goaf and the isolated coal pillar, increase the size of the coal pillar and avoid a high-stress concentration situation caused by lateral goaf.

2) Arrange the gap between tunnels to be at a reasonable distance

The gap between tunnels is an important factor in determining the stress applied to the coal seam in an isolated area. The geostatic stress and lateral abutment pressure from both sides of the tunnel can affect the coal pillar. Thus, increasing the gap

between tunnels can prevent the transfer of peak stress due to tunnel mining, reducing the degree of stress build-up and avoiding a rockburst.

3) Increase the compressive strength of the isolated area

According to **Eq. 14**, the probability for a rockburst is closely related to the uniaxial compressive strength of the coal. For a certain amount of stress applied to the coal, the smaller the uniaxial compressive strength, the higher is the probability for a rock burst, and vice versa. The grouting method can be used in a rock layer to increase the compressive strength or the tunnel can be set in a rock layer to increase strength, ensuring the tunnel and isolated area's long-term stability.

4) Increase the supporting strength of the tunnel and roof

An inspection of the scene of the rockburst in the current study reveals that the bolt mesh framework had failed and the roof support was bent, demonstrating that the existing support measures did not satisfy the requirements to prevent a rockburst. The bolt mesh framework and the roof support system must be strengthened.

5) Strengthening of monitoring and warning systems

An examination of microseismic and stress monitoring data associated with the rockburst reveals the occurrence of abnormal data. Thus, strengthening monitoring and warning systems, as well as implementing warning measures at both the local and global levels, are essential. When energy or stress levels increase abruptly, timely measures must be implemented to quickly release the pressure build-up to avoid rock bursts.

CONCLUSION

A mechanical model was established to investigate a tunnel-cut isolated coal seam, which was subject to lateral abutment pressure from goafs on both sides of the excavated zone. The model can be used to calculate the range affected by the goafs' stress. The lateral abutment pressure from goaf 302 caused stress concentration at a distance of 80–92 m. Because the goaf on the opposite side of the zone is far from the coal pillar, it cannot affect the isolated coal pillar.

Using numerical modeling, it was found that with tunnel cutting, the stability of the coal pillar decreased, and the isolated coal pillar was subject to a concentration of stress, causing the plastic area to decrease and the elastic area to increase. The lateral abutment pressure and geological conditions of the tunnel, as well as the working face, are the main factors that control the probability of a rockburst.

The following measures can be implemented to prevent a rockburst: 1) arrange a reasonable gap between the tunnel-cut isolated coal seam and the goafs; 2) arrange a reasonable gap between tunnels; 3) increase the compressive strength of isolated coal pillars; 4) strengthen mine support infrastructure; 5) strengthen the monitoring and warning systems installed in the mine.

The findings of this study can be used to assess the risk of rockburst for tunnel-cut isolated coal seams subjected to combine multiple stress fields.

DATA AVAILABILITY STATEMENT

The original contributions presented in the study are included in the article/supplementary material, further inquiries can be directed to the corresponding authors.

AUTHOR CONTRIBUTIONS

HZ: participation in the whole work; drafting of the article; TL, ZO, HY: checked and modified this paper; SL, HW: data analysis; JC, KL: provided technical guidance. All authors have read and agreed to the published version of the manuscript.

FUNDING

Financial supports from the National Natural Science Foundation of China, grant number: 51674016,52004090. Financial supports from the Natural Science Foundation of Hebei Province, grant number: E2020808025.

ACKNOWLEDGMENTS

Acknowledgements are also given to the support of Tianchi Hundred People Program of Xinjiang Uygur Autonomous Region (2019(39)) herein.

REFERENCES

Adoko, A. C., Gokceoglu, C., Wu, L., and Zuo, Q. J. (2013). Knowledge-based and Data-Driven Fuzzy Modeling for Rockburst Prediction. *Int. J. Rock Mech. Mining Sci.* 61, 86–95. doi:10.1016/j.ijrmms.2013.02.010

Barton, N., and Shen, B. (2017). Risk of Shear Failure and Extensional Failure Around Over-stressed Excavations in Brittle Rock. *J. Rock Mech. Geotechnical Eng.* 9, 210–225. doi:10.1016/j.jrmge.2016.11.004

Chen, S., Zhou, H., Guo, W., Wang, H., and Sun, X. (2012). Study on Long-Term Stress and Deformation Characteristics of Strip Pillar. *J. Min. Saf. Eng.* 29, 376–380.

Cui, L., Liu, Y., Sheng, Q., and Xiao, P. (2021). Experimental Study on Mechanical Properties and Cracking Behaviors of T-Shaped Flaw-Contained Rock-like Materials under Cyclic Loading. *Front. Earth. Sc-switz* 9. doi:10.3389/feart.2021.768077

Dou, L., He, Y., and Zhang, W. (2003). Hazards of Rock Burst in Island Coal Face and its Control. *Chin. J. Rock Mech. Eng.* 22, 1866–1869.

Fan, J., Jiang, D., Liu, W., Wu, F., Chen, J., and Daemen, J. (2019). Discontinuous Fatigue of Salt Rock with Low-Stress Intervals. *Int. J. Rock Mech. Mining Sci.* 115 (3), 77–86. doi:10.1016/j.ijrmms.2019.01.013

Fan, J., Liu, W., Jiang, D., Chen, J., William, N. T., Jaak, J. K., et al. (2020). Time Interval Effect in Triaxial Discontinuous Cyclic Compression Tests and Simulations for the Residual Stress in Rock Salt. *Rock Mech. Rock Eng.* (prepublish) 53, 4061–4076. doi:10.1007/s00603-020-02150-y

Feng, Y., Jiang, F., and Li, J. (2015). Evaluation Method of Rock Burst hazard Induced by Overall Instability of Island Coal Face. *J. China Coal Soc.* 40, 1001–1007. doi:10.13225/j.cnki.jccs.2014.0693

Jiang, D., Fan, J., Chen, J., Li, L., and Cui, Y. (2016). A Mechanism of Fatigue in Salt under Discontinuous Cycle Loading. *Int. J. Rock Mech. Mining Sci.* 86 (7), 255–260. doi:10.1016/j.ijrmms.2016.05.004

Jiang, D., Li, Z., Liu, W., Ban, F., Chen, J., Wang, Y., et al. (2021). Construction Simulating and Controlling of the two-well-Vertical(TWV) Salt Caverns with Gas Blanket. *J. Nat. Gas. Sci. Eng.* 96, 104291. doi:10.1016/j.jngse.2021.104291

Jiang, F., Cheng, G., Feng, Y., Wang, C., and Xu, Y. (2015). Research on Coal Overall Instability of Isolated Working Face with Irregular Gobs on Both Sides. *Chin. J. Rock Mech. Eng.* 34, 4164–4170.

Jiang, Y., Pan, Y., Jiang, F., Dou, L., and Ju, Y. (2014). State of the Art Review on Mechanism and Prevention of Coal Bumps in China. *J. China Coal Soc.* 39, 205–213. doi:10.13225/j.cnki.jccs.2013.0024

Jiang, Y., Song, H., Ma, Z., Ma, B., and Gao, L. (2018). Optimization Research on the Width of Narrow Coal Pillar along Goaf Tunnel in Tectonic Stress Zone. *J. China Coal Soc.* 43, 319–326. doi:10.13225/j.cnki.jccs.2017.4157

Kang, Y., Fan, J., Jiang, D., and Li, Z. (2021). Influence of Geological and Environmental Factors on the Reconsolidation Behavior of fine Granular Salt. *Nat. Resour. Res.* 30 (1), 805–826. doi:10.1007/s11053-020-09732-1

Keneti, A., and Sainsbury, B.-A. (2018). Review of Published Rockburst Events and Their Contributing Factors. *Eng. Geology.* 246, 361–373. doi:10.1016/j.enggeo.2018.10.005

Li, D., Liu, W., Jiang, D., Chen, J., Fan, J., and Qiao, W. (2021). Quantitative Investigation on the Stability of Salt Cavity Gas Storage with Multiple Interlayers above the Cavity Roof. *J. Energ. Storage.* 44, 103298. doi:10.1016/j.est.2021.103298

Li, D., Shi, X., Zhao, C., Ge, D., Chen, Y., Dong, C., et al. (2020). Mechanism of Rock Burst during Stope Mining with Interval Coal Pillar in One-Sided Mining Space. *J. Min. Saf. Eng.* 37, 1213–1221. doi:10.13545/j.cnki.jmse.2020.06.016

Li, Z., Dou, L., Wang, G., Cai, W., He, J., and Ding, Y. (2013). Rock Burst Characteristics and Mechanism Induced within an Island Pillar Coalface with Hard Roof. *Chin. J. Rock Mech. Eng.* 32, 333–342. doi:10.13545/j.issn1673-3363.2014.04.004

Liu, S., Bai, J., Wang, X., Wang, G., Wu, B., Li, Y., et al. (2021). Study on the Stability of Coal Pillars under the Disturbance of Repeated Mining in a Double-Roadway Layout System. *Front. Earth. Sc-switz.* 9 doi:10.3389/feart.2021.754747

Liu, W., Zhang, X., Fan, J., Zuo, J., Zhang, Z., and Chen, J. (2020a). Study on the Mechanical Properties of Man-Made Salt Rock Samples with Impurities. *J. Nat. Gas Sci. Eng.* 84, 103683. doi:10.1016/j.jngse.2020.103683

Liu, W., Zhang, Z., Fan, J., Jiang, D., Li, Z., and Chen, J. (2020b). Research on Gas Leakage and Collapse in the Cavern Roof of Underground Natural Gas Storage in Thinly Bedded Salt Rocks. *J. Energ. Storage* 31, 101669. doi:10.1016/j.est.2020.101669

Lu, S., and Guo, Y. (1991). The Relationship between the Width of Coal Pillar and the Deformation of Surrounding Rock. *J. China Univ. Min. Technol.* 04, 4–10.

Ma, T. H., Tang, C. A., Tang, L. X., Zhang, W. D., and Wang, L. (2015). Rockburst Characteristics and Microseismic Monitoring of Deep-Buried Tunnels for Jinping II Hydropower Station. *Tunnelling Underground Space Tech.* 49, 345–368. doi:10.1016/j.tust.2015.04.016

Pan, J., Ning, Y., Mao, D., Lan, H., Du, T., and Peng, Y. (2012). Theory of Rockburst Start-Up during Coal Mining. *Chin. J. Rock Mech. Eng.* 45, 1567–1584. doi:10.3969/j.issn.1000-6915.2012.03.017

Pan, Y., Li, Z., and Zhang, M. (2003). Distribution, Type, Mechanism, and Prevention of Rock Burst in China. *Chinj. Rock Mech. Eng.* 22, 1844–1851. doi:10.3321/j.issn:1000-6915.2003.11.019

Pinzani, A., and Coli, N. (2011). "A Practical Geostructural Approach for the Evaluation of Tunnel Water Inflow by Means of FEM Seepage Analysis," in Proceedings of the 45th US Rock Mechanics/Geomechanics Symposium, San Francisco, CA, USA, 26 June, 2011.

Qi, Q., Li, Y., Zhao, S., Zhang, N., Zheng, W., Li, H., et al. (2019). Seventy Years Development of Coal Mine Rockburst in China: Establishment and Consideration of Theory and Technology System. *Coal Sci. Technol.* 47, 1–40. doi:10.13199/j.cnki.cst.2019.09.001

Qi, Q., Pan, Y., Li, H., Jiang, D., ShuZhao, L. S., et al. (2020). Theoretical Basis and Key Technology of Prevention and Control of Coal-Rock Dynamic Disasters in Deep Coal Mining. *J. China Coal Soc.* 45, 1567–1584. doi:10.13225/j.cnki.jccs.DY20.0453

Rehman, H., Naji, A. M., Nam, K., Ahmad, S., Muhammad, K., and Yoo, H.-K. (2021). Impact of Construction Method and Ground Composition on Headrace Tunnel Stability in the Neelum-Jhelum Hydroelectric Project: A Case Study Review from Pakistan. *Appl. Sci.* 11, 1655. doi:10.3390/app11041655

Song, Y., Pan, Y., Li, Z., and Yin, W. (2018). Creep Instability of Isolated Coal Pillar under Rock Burst. *Saf. Coal Mines.* 49, 47–50. doi:10.13347/j.cnki.mkaq.2018.05.012

Tian, Y., Wu, Y., Li, H., Ren, B., and Wang, H. (2021). Earthquake Dynamic Failure Mechanism of Dangerous Rock Based on Dynamics and PFC3D. *Front. Earth. Sc-switz.* 9 doi:10.3389/feart.2021.683193

Wang, C., Jiang, F., Wang, P., Kong, L., Sun, Q., and Sun, C. (2009). Microseismic Events Distribution Characteristics and Mechanical Mechanisms of Rock Bursting Induced by a Coal Pillar. *J. China Coal Soc.* 34, 1169–1173.

Wang, G., Zhu, S., Jiang, F., Wang, B., Zhou, T., Zuo, E., et al. (2019). Mechanism of Rock Burst Induced by Overall Instability of Isolated Coal and its Prevention in Large Well at Thousands-Kilometer Underground. *J. Min. Saf. Eng.* 36, 968–976. doi:10.13545/j.cnki.jmse.2019.05.014

Wang, L., and Miao, X. (2007). Study on Catastrophe Characteristics of the Destabilization of Coal Pillars. *J. China Univ. Min. Technol.* 01, 7–11.

Wu, Z., Pan, P., Chen, J., Liu, X., Miao, S., and Yu, P. (2021). Mechanism of Rock Bursts Induced by the Synthetic Action of "Roof Bending and Rock Pillar Prying" in Subvertical Extra-thick Coal Seams. *Front. Earth. Sc-switz.* 9 doi:10.3389/feart.2021.737995

Xiong, Z., Liu, W., Jiang, D., Qiao, W., Liu, E., Zhang, N., et al. (2021). Investigation on the influences of interlayer contents on stability and usability of energy storage caverns in bedded rock salt. *Energy.* doi:10.1016/j.energy.2021.120968

Xu, J., Jiang, J., Xu, N., Liu, Q., and Gao, Y. (2017). A New Energy index for Evaluating the Tendency of Rockburst and its Engineering Application. *Eng. Geology.* 230, 46–54. doi:10.1016/j.enggeo.2017.09.015

Yang, Y., Duan, H., Liu, C., and Hao, Y. (2017). Reasonable Design of Coal Barrier Pillar of Roadway in Deep Mining Considering Long-Term Stability. *J. Min. Saf. Eng.* 34, 921–927. doi:10.13545/j.cnki.jmse.2017.05.014

Yin, W., Zan, D., and Nie, S. (2012). The Coal Pillar Dimensions of the Gathering Dip in a Joint Disposed District. *Chin. Coal.* 38, 45–48. doi:10.19880/j.cnki.ccm.2012.01.011

Zhang, H., Tang, Y., Okubo, S., Peng, S., and Chen, C. (2021b). Generalized Relaxation Behavior of Rock under Various Loading Conditions Using a Constant Linear Combination of Stress and Strain. *Front. Earth. Sc-switz.* 9 doi:10.3389/feart.2021.769621

Zhang, X., Liu, W., Jiang, D., Qiao, W., Liu, E., Zhang, N., et al. (2021a). Investigation on the Influences of Interlayer Contents on Stability and Usability of Energy Storage Caverns in Bedded Rock Salt. *Energy* 231, 120968. doi:10.1016/j.energy.2021.120968

Zhao, B., Wang, F., Liang, N., and Wang, W. (2018). Reasonable Segment Pillar Width and its Control Technology for Fully Mechanized Top-Coal Caving Face with High Stress. *J. Min. Saf. Eng.* 35, 19–26. doi:10.13545/j.cnki.jmse.2018.01.003

Zheng, X., Yao, Z., and Zhang, N. (2012). Stress Distribution of Coal Pillar with Gob-Side Entry Driving in the Process of Excavation and Mining. *J. Min. Saf. Eng.* 29, 459–465.

Zhou, J., Li, X., and Mitri, H. S. (2018). Evaluation Method of Rockburst: State-Of-The-Art Literature Review. *Tunnelling Underground Space Tech.* 81, 632–659. doi:10.1016/j.tust.2018.08.029

Conflict of Interest: Authors JC and KL were employed by the company Shenhua Xinjiang Energy Co., Ltd.

The remaining authors declare that the research was conducted in the absence of any commercial or financial relationships that could be construed as a potential conflict of interest.